ACS APPLIED MATERIALS & INTERFACES

Research Article

Cite This: ACS Appl. Mater. Interfaces 2019, 11, 13984−13990

www.acsami.org

Micropatterned Viral Membrane Clusters for Antiviral Drug Evaluation

Soohyun Park,[†,§] Joshua A. Jackman,[‡,§] Xiaobin Xu,[§,⊥,#] Paul S. Weiss,[§,⊥] and Nam-Joon Cho*[,†,§,∥]

[†]School of Materials Science and Engineering, Nanyang Technological University, 50 Nanyang Drive, Singapore 637553, Singapore

[‡]School of Chemical Engineering and [§]SKKU-UCLA-NTU Precision Biology Research Center, Sungkyunkwan University, Suwon 16419, Republic of Korea

[∥]School of Chemical and Biomedical Engineering, Nanyang Technological University, 62 Nanyang Drive, Singapore 637459, Singapore

[⊥]California NanoSystems Institute, Department of Chemistry and Biochemistry, and Department of Materials Science and Engineering, University of California, Los Angeles, Los Angeles, California 90095-7227, United States

[#]School of Materials Science and Engineering, Tongji University, 1239 Siping Road, Shanghai 200092, China

Supporting Information

ABSTRACT: The function of biological nanoparticles, such as membrane-enveloped viral particles, is often enhanced when the particles form higher-order supramolecular assemblies. While there is intense interest in developing biomimetic platforms that recapitulate these collective properties, existing platforms are limited to mimicking individual virus particles. Here, we present a micropatterning strategy to print linker molecules selectively onto bioinert surfaces, thereby enabling controlled tethering of biomimetic viral particle clusters across defined geometric patterns. By controlling the linker concentration, it is possible to tune the density of tethered particles within clusters while enhancing the signal intensity of encapsulated fluorescent markers. Time-resolved tracking of pore formation and membrane lysis revealed that an antiviral peptide can disturb clusters of the membrane-enclosed particles akin to the targeting of individual viral particles. This platform is broadly useful for evaluating the performance of membrane-active antiviral drug candidates, whereas the micropatterning strategy can be applied to a wide range of biological nanoparticles and other macromolecular entities.

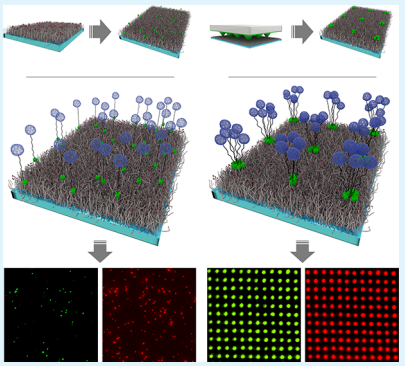

KEYWORDS: *micropatterning, nanotechnology, nanoparticles, biomaterials, self-assembly, virus*

INTRODUCTION

The development of highly parallel, surface-based experimental platforms to investigate nanoscopic liposomes and other biological nanoparticles such as exosomes and viruses has opened the door to understanding a wide range of membrane-related chemical reactions,[1,2] enzymatic processes,[3] and biophysical activities.[4] One particularly useful measurement platform involves the site-specific tethering of well-separated liposomes for real-time monitoring of biomacromolecular interaction processes via fluorescence[5] or scattering[6,7] microscopy techniques. These tethering strategies mimic those used for selective molecular capture surfaces using chemically functionalized surfaces.[8−12] Likewise, the liposomes are synthetic, spherical lipid bilayer nanoparticles that mimic the architecture of complex biological nanoparticles such as membrane-enveloped viruses while providing a well-controlled platform to investigate dynamic membrane interactions. Importantly, each individual liposome can be studied in parallel, which overcomes challenges with ensemble averaging and enables insights with high statistical significance.[13,14]

Using a two-fluorophore system to simultaneously track membrane permeation and lysis, time-lapsed fluorescence microscopy experiments revealed that membrane curvature beyond a certain threshold triggers the formation of pores in individual, enveloped virus-mimicking liposomes by an amphipathic, α-helical (AH) peptide.[15] Following similar experimental approaches, it was later discovered that the membrane curvature sensing exhibited by this AH peptide is rather unique compared to that of other antiviral peptides[16] and peptide engineering could further modulate the degree of membrane curvature sensing.[17] Furthermore, the AH peptide has been shown to exhibit similar membrane-disruptive behavior against zwitterionic, positively charged, and negatively charged liposomes.[18] Importantly, the biophysical findings obtained with virus-mimicking model liposomes were translated into a novel therapeutic strategy called lipid envelope

Received: January 26, 2019
Accepted: March 11, 2019
Published: March 11, 2019

DOI: 10.1021/acsami.9b01724
ACS Appl. Mater. Interfaces 2019, 11, 13984−13990

antiviral disruption (LEAD), whereby an engineered AH peptide was demonstrated to inhibit viral particles in vivo.[17]

There is intense interest in understanding how biological nanoparticles, such as viruses, form cooperative assemblies with heightened functionalities.[19] One of the most important examples concerns cellular infection by viral particles. Oftentimes, individual viral particles have relatively low infection efficiencies, whereas clusters of viral particles can display greater infectivity levels.[20,21] Interestingly, this cooperative activity has evolved independently across multiple viral families.[22] Cooperative assemblies (termed "clusters" here) can consist of aggregates of viral particles alone[23] or enclosed within vesicular bodies.[24,25] Other evidence also points to the importance of viral particle clusters, such as the observation that amyloid fibrils can enhance sexual transmission of numerous viruses by inducing aggregation of viral particles.[26] Indeed, it has long been recognized that it is difficult to neutralize clusters of viral particles[27] and clusters can also exhibit high environmental stability.[28] Altogether, these findings underscore the importance of developing therapeutic strategies aimed at targeting clustered viral particles.

To date, however, existing measurement platforms have focused on tethering individual liposomes in nonclustered formats, whereas the nonspecific adsorption of liposomes in close-packed adlayers is limited to ensemble-averaged readouts. The development of a measurement platform that mimics the architectural configuration of clustered viral particles, i.e., collections of nanoscopic, membrane-enclosed objects in grouped arrays, enables cluster-by-cluster measurement analysis and would greatly facilitate mechanistic understanding of how the LEAD strategy can be deployed against viral clusters and other aggregates of biological nanoparticles (Figure 1).

MATERIALS AND METHODS

Reagents. Lipids were obtained from Avanti Polar Lipids (Alabaster, AL), which were received in either chloroform solution or powder form. Lipids included 1,2-dioleoyl-*sn*-glycero-3-phosphocholine (DOPC), 1,2-distearoyl-*sn*-glycero-3-phosphoethanolamine-*N*-[biotinyl(polyethylene glycol)-2000] (ammonium salt) (DSPE-PEG(2000)biotin), and 1,2-dioleoyl-*sn*-glycero-3-phosphoethanolamine-*N*-(lissamine rhodamine B sulfonyl) (ammonium salt) (Rh-PE). The Rh-PE lipid is a fluorescently labeled lipid, whereby the lissamine rhodamine B sulfonyl probe is covalently conjugated to the phosphoethanolamine headgroup. All reagents were mixed in chloroform to the desired molar ratio as part of the liposome preparation, as described below. An amphipathic, α-helical (AH) peptide (SGSWLRDVWDWICTVLTDFKTWLQSKL-NH_2) was synthesized by and obtained from AnaSpec Corporation (Fremont, CA). The lyophilized peptide was first solubilized in 4% dimethyl sulfoxide (DMSO > 99.9%) and then diluted with deionized water to prepare a stock solution (2 mg/mL). Molar concentrations were measured by standard absorbance measurements at 280 nm.[29] The buffer used in all experiments was 10 mM Tris buffer with 150 mM NaCl (pH 7.5). Buffers and solutions were prepared with Milli-Q-treated water (MilliporeSigma, Burlington, MA).

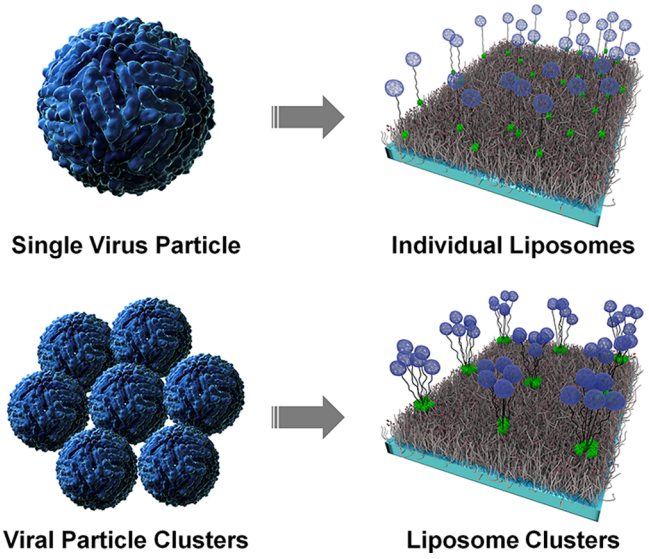

Figure 1. Schematic illustration of the experimental strategy. Micropatterned viral membrane clusters mimic the architecture of viral particle clusters, which often display heightened functionality compared to that of individual particles. The clusters consist of enveloped virus-mimicking liposomes akin to viral particle aggregates.

Liposome Preparation. Small unilamellar liposomes were prepared by an extrusion method, as previously described.[30] The lipid composition was 99.2 mol % DOPC, 0.7 mol %, Rh-PE, and 0.1 mol % DSPE-PEG(2000)biotin. Briefly, lipids dissolved in chloroform were first dried under a gentle stream of nitrogen air at room temperature and then stored under vacuum overnight to remove residual chloroform. The dried lipids were hydrated in a buffer solution containing 14.3 mM calcein, followed by seven cycles of freeze−thaw treatment to increase the encapsulation efficiency and unilamellarity. Then, the lipid suspension was passed through 50 nm diameter pore, track-etched polycarbonate membranes a total of 21 times by a MiniExtruder (Avanti Polar Lipids). Liposome suspensions were diluted immediately before experiment to 0.2 mg/mL, and free calcein was removed by a Sephadex G-25 gel filtration column (GE Healthcare Life Sciences, Pittsburgh, PA). After liposome preparation, the size distribution of extruded liposomes was obtained by dynamic light scattering with a ZetaPals particle size analyzer (Brookhaven Instruments, Holtsville, NY).

PDMS Stamp Fabrication. A SiO_2 film (500 nm) was thermally grown on a Si(100) wafer. Conventional photography was performed to generate a pattern of a 2D array of squares (2 μm in length and 3.5 μm pitch) on the photoresist coated on the SiO_2/Si(100) wafer. After that, the exposed SiO_2 was selectively etched by reactive ion etching (Oxford 80 Plus) using a gas mixture of CHF_3 (25 sccm) and Ar (25 sccm) at 35 mTorr. Next, the exposed Si(100) was anisotropically etched in a mixture of 4:1 KOH (30%) and isopropanol at 75 °C to generate a 2D array of recessed pyramidal structures. After removing the remaining SiO_2 and photoresists in a 25% HF solution for 5 min, Si masters with recessed pyramidal structures were obtained. Next, the Sylgard 184 elastomer silicone elastomer base and a curing agent (in a mass ratio of 10:1) were well mixed, degassed, poured onto the Si masters, and cured at 65 °C overnight. After curing, poly(dimethylsiloxane) stamps carrying a 2D array of pyramidal structures were formed and then they were carefully peeled off from the Si master.

Microcontact Printing (μCP). Glass microscope coverslips and poly(dimethylsiloxane) (PDMS) stamps were cleaned by 1 wt % sodium dodecyl sulfate (SDS), deionized water, and ethanol in sequence, followed by 30 s of oxygen plasma treatment (Harrick Plasma, Ithaca, NY) to render the surface hydrophilic and remove residual organic contaminants. Then, the glass substrate was coated with poly(L-lysine)-grafted poly(ethylene glycol)-biotin (PLL-*g*-PEG-biotin 50%, SuSoS AG, Dübendorf, Switzerland, 41.7 μg/mL diluted in buffer solution). The stamp was immersed with a few drops (15−20 μL) of stamping solution (ink containing defined neutravidin protein concentrations) for 5 min. Then, the stamp was dried by inert nitrogen gas and placed in contact with the coverslip for a few seconds to transfer neutravidin onto the biotinylated glass surface. Of note, the time interval between drying the ink on the stamp and ink printing was kept as short as possible because the transfer success decreases significantly after 1 min of drying.[31] Then, a sticky-slide $VI^{0.4}$ (ibidi

DOI: 10.1021/acsami.9b01724
ACS Appl. Mater. Interfaces 2019, 11, 13984−13990

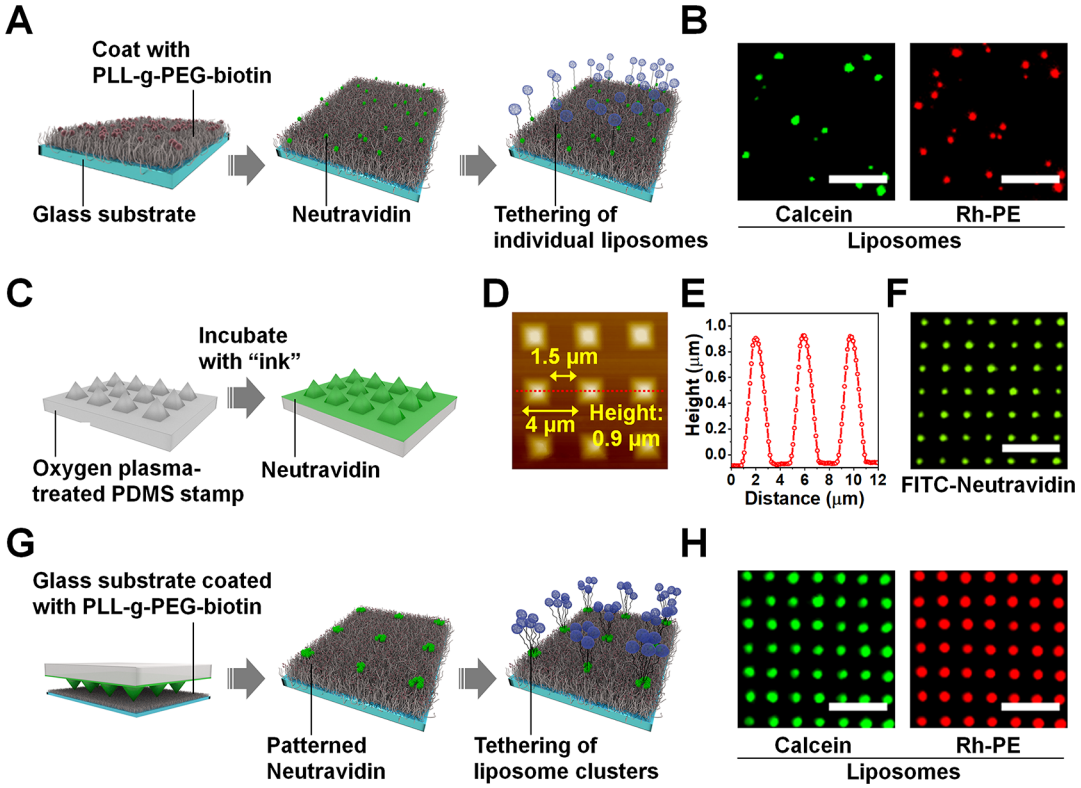

Figure 2. Design of the viral membrane cluster platform. (A) Schematic illustration of tethering individual liposomes. (B) Fluorescence microscope images of individually tethered liposomes (~100 nm diameter), as indicated by calcein and rhodamine signals. (C) Schematic illustration describing microcontact printing (μCP) for location-specific patterning of neutravidin protein molecules. (D) Atomic force microscope (AFM) image of a poly(dimethylsiloxane) (PDMS) stamp with a pyramidal stamp pattern. (E) Height profile from the AFM scan corresponding to the PDMS stamp shown in (D). (F) Fluorescence microscope images of FITC-labeled neutravidin on a bare glass substrate. (G) Schematic illustration describing the μCP strategy to form micropatterned viral membrane clusters. (H) Fluorescence microscope images of patterned liposomes on a PLL-*g*-PEG/PLL-*g*-PEG-biotin functionalized glass surface, as indicated by calcein and rhodamine signals. All scale bars are 10 μm.

GmbH, Martinsried, Germany) was attached onto the stamped coverslip to form a microfluidic chamber. Then, each chamber was washed with more than 2 mL of buffer prior to 5 min incubation with 0.025 μg/mL biotinylated liposomes. As for the control experiments with nonpatterned samples, all procedures were the same, except neutravidin was incubated directly in the microfluidic chamber for 20 min.

Epifluorescence Microscopy. Imaging experiments were conducted using a Nikon Eclipse Ti-E inverted microscope with a 60× oil-immersion objective (NA 1.49). The excitation source was a C-HGFIE Intensilight mercury fiber illuminator (Nikon, Tokyo, Japan), and the light was passed through an alternating dichroic filter block (Ex 480/40, Em 535/50) or (Ex 545/30, Em 605/70) for imaging in the FITC and TRITC channels, respectively. An Andor iXon3 897 EMCCD camera was used to obtain the images at the rate of 1 frame per 24 s in four neighboring spots, respectively, to minimize thermal drift and loss of focus. The experimental substrate was enclosed within a microfluidic chamber, and the liquid sample was introduced at a flow rate of 100 μL/min, as controlled by a peristaltic pump (model no. ISM833C, Ismatec, Wertheim, Germany).

RESULTS AND DISCUSSION

We begin by reconfiguring the tethered liposome platform to accommodate clusters of virus-mimetic liposomes in organized arrangements. Conventionally, tethered liposomes contain a small fraction of biotinylated lipid and are attached to biotin moieties on a PLL-*g*-PEG/PLL-*g*-PEG-biotin-functionalized[32] glass surface via neutravidin coupling (Figure 2A). In this case, a bulk solution of neutravidin is first incubated with the functionalized surface, and neutravidin molecules bind universally across the surface to biotin moieties, and then the biotinylated liposomes are added for subsequent coupling in a sandwich configuration. Individual liposomes can be identified by epifluorescence microscopy, whereby water-soluble calcein molecules (green fluorescence) are encapsulated within the liposomal interior and rhodamine-labeled phospholipids (red fluorescence) form part of the liposomal bilayer (Figure 2B). Hence, drops in the calcein and rhodamine signals can indicate membrane permeation and lysis, respectively.

We extend these basic sensing principles to develop a hierarchically assembled cluster platform by employing microcontact printing (μCP).[31,33] The strategy is based on fabricating a poly(dimethylsiloxane) (PDMS) stamp with precisely fabricated relief structures that define a printing pattern (Figure 2C). The PDMS stamp was rendered hydrophilic by oxygen plasma treatment and coated with a neutravidin "ink" that can be printed onto target surfaces in patterns defined by the relief features on the stamp. Atomic force microscopy measurements indicate that the PDMS stamp consists of equidistantly spaced, pyramidal tips with heights and widths of 0.9 and 2 μm, respectively, and a separation distance of 1.5 μm between nearest-neighbor edges, as defined lithographically into the master from which the stamp was produced (Figure 2D,E). These geometrical dimensions are suitable for robust printing, as demonstrated by the controlled printing of fluorescently labeled neutravidin on a bare glass surface (Figure 2F).

DOI: 10.1021/acsami.9b01724
ACS Appl. Mater. Interfaces 2019, 11, 13984−13990

Using unlabeled neutravidin (10 μg/mL), the μCP strategy was next applied to a PLL-*g*-PEG/PLL-*g*-PEG-biotin-functionalized glass surface (Figure 2G). The functionalized glass surface was treated with the neutravidin-coated PDMS stamp to immobilize neutravidin molecules selectively, in the target regions only. Each contacting substrate was well hydrated to ensure effective transfer of neutravidin molecules from a nonspecific adsorbed state on the PDMS stamp to being captured by biotin moieties on the functionalized glass surface. Whereas μCP methods typically involve physical deposition or prefunctionalization,[34] the selective transfer of neutravidin in our case is more elaborate because the protein molecules are being transferred to a nominally bioinert surface and the specific attachment is mediated by biotin moieties, with the latter functionalization occuring after deposition. This distinction is important because our approach enables the subsequent attachment of high densities of fluorescently labeled liposomes in neutravidin-printed regions, whereas other surrounding regions are devoid of liposomes, as confirmed by epifluorescence microscopy (Figure 2H). Both the rhodamine and calcein signals indicate that the tethered liposomes faithfully mimic the chemical pattern, pointing to the successful formation of a measurement platform comprising clusters of virus-mimetic liposomes. Compared with the nonpatterned platform, the μCP strategy also overcomes the incubation time and reagent concentration requirements of diffusion-limited attachment schemes, thereby enabling efficient transfer with minimal reagents in a small volume.

We next systematically investigated how varying the amount of bound neutravidin can influence the formation of virus-mimetic clusters, as presented in Figure 3. The experiments were conducted in comparative fashion across the micropatterned cluster and conventional, nonpatterned platforms; liposomes of ~62 nm diameter were detected by the calcein and rhodamine signals (Figure S1). The reported neutravidin concentrations correspond to the bulk protein concentration that was used during the appropriate platform fabrication step. In the absence of neutravidin, there was negligible liposome immobilization on either platform, consistent with the nonfouling characteristics of the PLL-*g*-PEG/PLL-*g*-PEG-biotin layer.

With 0.1 μg/mL neutravidin, trace liposomes were immobilized on the nonpatterned platform, whereas some clusters were formed on the micropatterned platform. Notably, the clusters exhibited wide variances in fluorescence intensities and were irregularly distributed across the surface. With 1 μg/mL neutravidin, there were greater densities of immobilized liposomes on the nonpatterned platform, although appreciably more liposomes were detected within the same field of view by the rhodamine signal than the calcein signal. We attribute this difference to the small liposome size and the resulting low amount of encapsulated calcein molecules.[35] Likewise, clusters on the micropatterned platform began to assume more uniform characteristics, as indicated by the correlation of the cluster location with the designed chemical pattern. However, there were still high variances in the fluorescence intensities per cluster, especially for the calcein signal.

For the nonpatterned platform, similar trends were observed with 10 μg/mL neutravidin and there were high densities of immobilized liposomes, albeit the number of liposomes detected by the rhodamine signal was appreciably higher than the number detected by the calcein signal. In contrast, cluster formation on the patterned platform exhibited high

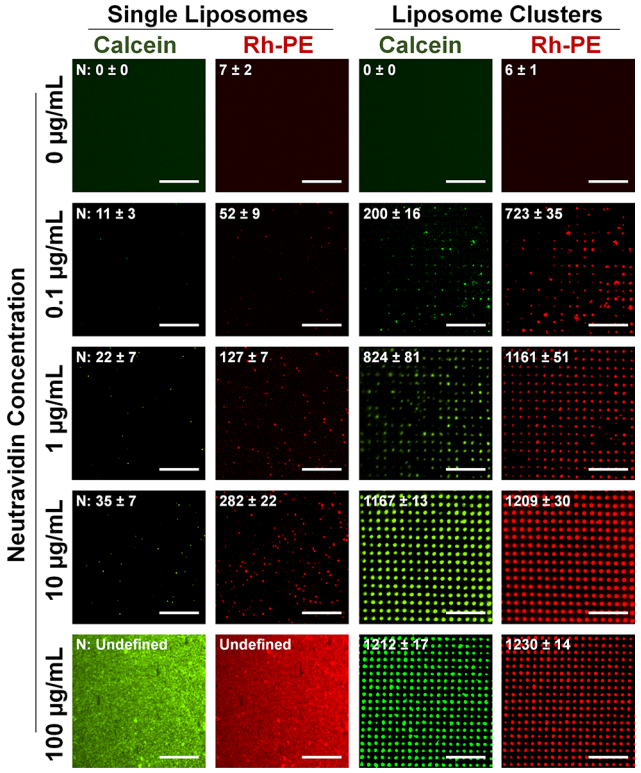

Figure 3. Fluorescent microscope images comparing immobilization of tethered liposomes in single-liposomes and clustered liposome arrangements. The calcein and rhodamine signals are presented for each experimental set. During fabrication, the bulk neutravidin concentration was varied from 0 to 100 μg/mL to control the density of tethered liposomes. The number of tethered liposomes or clusters identified by the calcein or rhodamine signals is reported in the upper right image and is based on imaging in 10 different fields of view. For the nonpatterned platform, it was not possible to quantify the number of individual liposomes for the 100 μg/mL neutravidin case. All scale bars are 20 μm.

degrees of uniformity, as indicated by cluster locations as well as more similar numbers of clusters being detected by the calcein and rhodamine signals (Figures S2 and S3). The intensity values were also higher than those obtained with lower neutravidin concentrations, indicating that greater densities of liposomes were immobilized per cluster. On the other hand, with 100 μg/mL neutravidin, nearly complete saturation of the surface was observed with the nonpatterned platform. Whereas a granular appearance in the fluorescence microscopy images suggests the presence of immobilized liposomes, the high density of immobilized liposomes obfuscates intensity quantification. In marked contrast, the patterned platform had nearly uniform clusters across the entire surface and each cluster could be discerned individually. In general, the fluorescence intensity within the printed spots on the patterned platform was higher than the fluorescence intensity of individual liposomes on the nonpatterned platform. The increased fluorescence intensity is likely related to a higher surface density of tethered liposomes within the spots and consistent with the high neutravidin densities that can be achieved using the quick and efficient μCP process,[36] as compared to the conventional diffusion-limited attachment of neutravidin molecules across the entire substrate. In other works, we have shown the advantages of building spatially encoded internal controls into such measurements.[37,38]

DOI: 10.1021/acsami.9b01724
ACS Appl. Mater. Interfaces 2019, 11, 13984−13990

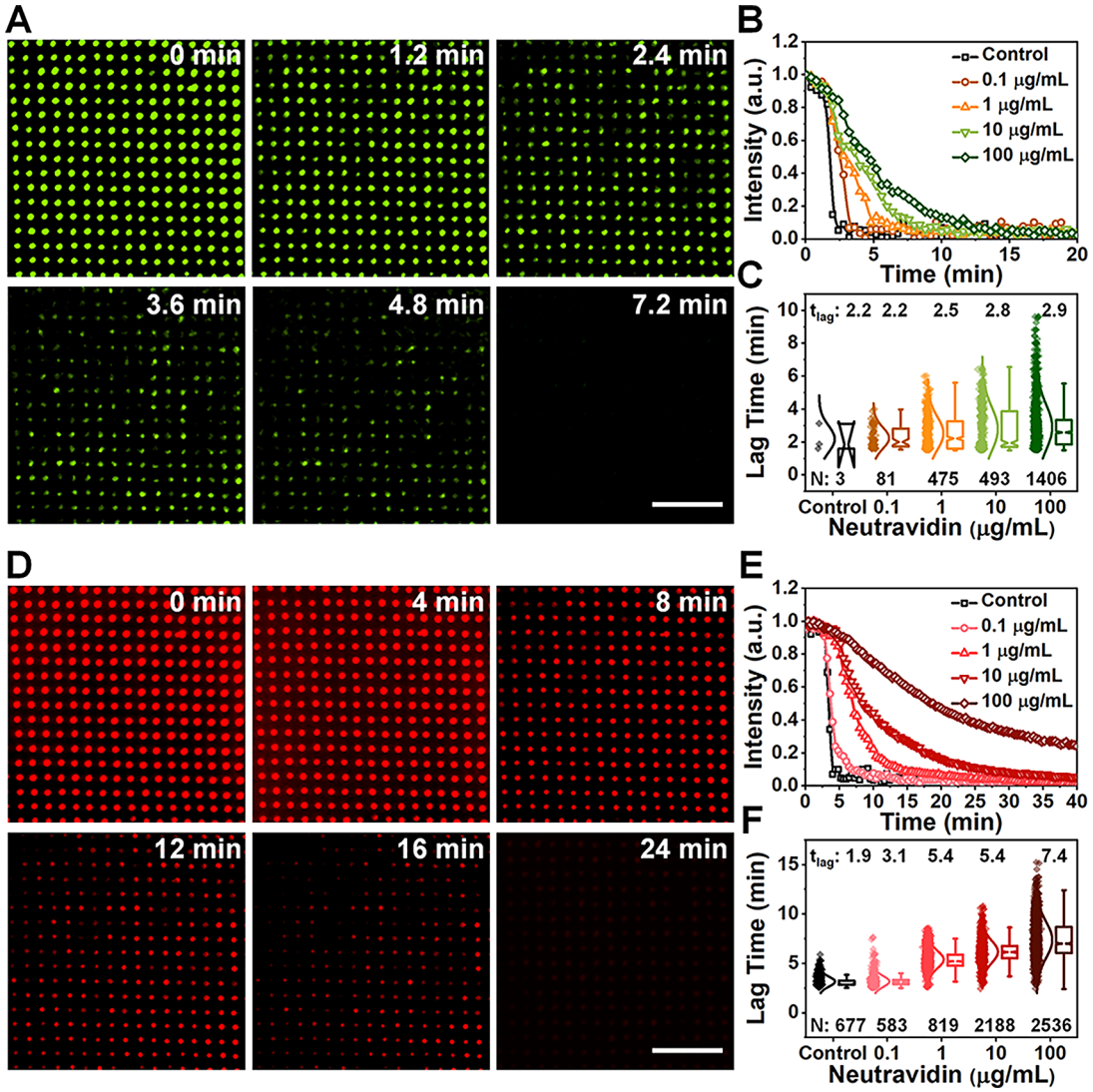

Figure 4. Time-resolved tracking of AH peptide interaction with micropatterned viral membrane clusters. (A) Time-lapse fluorescent microscope images show the change in calcein signal when 100 nM AH peptide was added to clusters at t = 0 min. During fabrication, the bulk neutravidin concentration was 10 μg/mL. (B) Changes in the normalized calcein signal intensity of a representative, individual cluster for platforms fabricated using different neutravidin concentrations with the time-resolved release of the calcein marker. (C) Box plot graph reporting trend in calcein release times. Data correspond to experiments presented in (B). Each dot represents one cluster, and mean values are reported from Gaussian fitting. (D–F) Corresponding data are presented for the rhodamine signal in the same experimental series. All scale bars are 20 μm. Control indicates the nonpatterned platform that was fabricated using a 10 μg/mL neutravidin concentration.

We next investigated the interaction of 100 nM AH peptide with micropatterned virus-mimetic clusters prepared using different neutravidin concentrations, hence varying liposome densities within individual clusters. Peptide-induced pore formation was investigated by tracking changes in the calcein signal. Representative time-lapsed micrographs for the 10 μg/mL neutravidin case are presented in Figure 4A, and the time-dependent drop in the calcein signal per cluster indicates that the AH peptide is capable of causing membrane permeabilization in clustered liposomes. Indeed, the AH peptide-induced complete release of encapsulated calcein across all tested cluster densities (Figure 4B). With the increasing neutravidin concentration, the time scale of complete calcein release was slower, supporting that the AH peptide likely takes a longer time to penetrate the entire cluster of liposomes due to hindered diffusion of peptide molecules through and around the barrier-like liposomes, as compared to diffusion through the bulk solution.[39,40] The AH peptide selectively forms pores in small (high-curvature) liposomes,[41,42] reinforcing that the ~62 nm diameter liposomes maintain their individual architectures within the collective assembly. Of note, the onset of calcein release was only weakly dependent on the neutravidin concentration, consistent with the outer liposomes being permeabilized more quickly than liposomes within the cluster (Figure 4C).

In addition to tracking pore formation, membrane lysis by the AH peptide was further interrogated by monitoring the rhodamine signal. Representative time-lapsed micrographs for the 10 μg/mL neutravidin case are presented in Figure 4D. The progressive decrease in the fluorescence intensity of individual clusters indicates that the AH peptide causes complete membrane lysis. Across the range of tested neutravidin concentrations, the AH peptide-induced drops in the rhodamine signal (Figure 4E). Up to 10 μg/mL neutravidin, the AH peptide caused complete membrane lysis of the clusters, whereas incomplete lysis occurred at

DOI: 10.1021/acsami.9b01724
ACS Appl. Mater. Interfaces 2019, 11, 13984–13990

100 μg/mL neutravidin-generated patterns. The latter finding supports that the AH peptide is effective at disrupting clusters up to a certain liposome density, but the rupture efficiency becomes lower at higher liposome densities. With the increasing neutravidin concentration, the time scale of liposome rupture also becomes longer (Figure 4F). This trend presumably relates to the greater number of tethered liposomes along with the higher density of liposomes within each individual cluster.

CONCLUSIONS

In summary, we have demonstrated that virus-mimetic clusters of tethered liposomes can be assembled using microcontact printing. This platform has significant advantages over conventional single-liposome arrays in terms of material requirements, fabrication speed, and control over platform architecture. Following this approach, one can track the time-resolved interactions between individual clusters and a membrane-disrupting antiviral peptide, revealing how viral particle clusters are susceptible to peptide treatment. This cluster platform is particularly representative of viral particle aggregates, while other types of clusters exist, including one in which a giant vesicle cloaks aggregated viral particles. Since it is known that the AH peptide can translocate the lipid bilayer of giant unilamellar vesicles,[43] it will be interesting to extend these studies to in vitro experimental settings to determine how the results obtained with this engineering platform correlate with a drug's inhibitory activity against viral particle aggregates and/or giant vesicle-cloaked viral particle assemblies. Such insights complement the insights obtained using conventional single-liposome arrays and open the door to understanding the biochemical and biophysical interactions involving clusters of biological nanoparticles such as viruses. In a future work, these measurement capabilities will also be useful for further exploring how membrane factors such as lipid composition influence the activity profile of antiviral drug candidates targeting viral particle clusters.

ASSOCIATED CONTENT

Supporting Information

The Supporting Information is available free of charge on the ACS Publications website at DOI: 10.1021/acsami.9b01724.

Dynamic light scattering measurements (Figure S1), fluorescence intensity quantification of liposome clusters (Figure S2), and quantification of tethered liposomes on nonpatterned and patterned platforms (Figure S3) (PDF)

AUTHOR INFORMATION

Corresponding Author

*E-mail: njcho@ntu.edu.sg.

ORCID

Soohyun Park: 0000-0003-3261-7585
Joshua A. Jackman: 0000-0002-1800-8102
Xiaobin Xu: 0000-0002-3479-0130
Paul S. Weiss: 0000-0001-5527-6248
Nam-Joon Cho: 0000-0002-8692-8955

Notes

The authors declare no competing financial interest.

ACKNOWLEDGMENTS

This work was supported by the National Research Foundation of Singapore through a Competitive Research Programme grant (NRF-CRP10-2012-07) and a Proof-of-Concept grant (NRF2015NRF-POC0001-19). Additional support was provided by the Creative Materials Discovery Program through the National Research Foundation of Korea funded by the Ministry of Science, ICT and Future Planning (NRF-2016M3D1A1024098). The fabrication was supported by a (US) National Science Foundation Nanomanufacturing grant #CMMI-1636136.

REFERENCES

(1) Bolinger, P. Y.; Stamou, D.; Vogel, H. An Integrated Self-Assembled Nanofluidic System for Controlled Biological Chemistries. *Angew. Chem., Int. Ed.* **2008**, *47*, 5544−5549.

(2) Christensen, S. M.; Bolinger, P.-Y.; Hatzakis, N. S.; Mortensen, M. W.; Stamou, D. Mixing Subattolitre Volumes in a Quantitative and Highly Parallel Manner with Soft Matter Nanofluidics. *Nat. Nanotechnol.* **2012**, *7*, 51.

(3) Rabe, M.; Tabaei, S. R.; Zetterberg, H.; Zhdanov, V. P.; Höök, F. Hydrolysis of a Lipid Membrane by Single Enzyme Molecules: Accurate Determination of Kinetic Parameters. *Angew. Chem.* **2015**, *127*, 1036−1040.

(4) Flagmeier, P.; De, S.; Wirthensohn, D. C.; Lee, S. F.; Vincke, C.; Muyldermans, S.; Knowles, T. P.; Gandhi, S.; Dobson, C. M.; Klenerman, D. Ultrasensitive Measurement of Ca^{2+} Influx into Lipid Vesicles Induced by Protein Aggregates. *Angew. Chem., Int. Ed.* **2017**, *56*, 7750−7754.

(5) Stamou, D.; Duschl, C.; Delamarche, E.; Vogel, H. Self-Assembled Microarrays of Attoliter Molecular Vessels. *Angew. Chem.* **2003**, *115*, 5738−5741.

(6) Andrecka, J.; Spillane, K. M.; Ortega-Arroyo, J.; Kukura, P. Direct Observation and Control of Supported Lipid Bilayer Formation with Interferometric Scattering Microscopy. *ACS Nano* **2013**, *7*, 10662−10670.

(7) Agnarsson, B. R.; Lundgren, A.; Gunnarsson, A.; Rabe, M.; Kunze, A.; Mapar, M.; Simonsson, L.; Bally, M.; Zhdanov, V. P.; Höök, F. Evanescent Light-Scattering Microscopy for Label-Free Interfacial Imaging: From Single Sub-100 nm Vesicles to Live Cells. *ACS Nano* **2015**, *9*, 11849−11862.

(8) Vaish, A.; Shuster, M. J.; Cheunkar, S.; Singh, Y. S.; Weiss, P. S.; Andrews, A. M. Native Serotonin Membrane Receptors Recognize 5-Hydroxytryptophan-functionalized Substrates: Enabling Small-molecule Recognition. *ACS Chem. Neurosci.* **2010**, *1*, 495−504.

(9) Hou, S.; Zhao, H.; Zhao, L.; Shen, Q.; Wei, K. S.; Suh, D. Y.; Nakao, A.; Garcia, M. A.; Song, M.; Lee, T.; et al. Capture and Stimulated Release of Circulating Tumor Cells on Polymer-grafted Silicon Nanostructures. *Adv. Mater.* **2013**, *25*, 1547−1551.

(10) Im, H.; Shao, H.; Park, Y. I.; Peterson, V. M.; Castro, C. M.; Weissleder, R.; Lee, H. Label-free Detection and Molecular Profiling of Exosomes with a Nano-Plasmonic Sensor. *Nat. Biotechnol.* **2014**, *32*, 490.

(11) Jackman, J. A.; Linardy, E.; Yoo, D.; Seo, J.; Ng, W. B.; Klemme, D. J.; Wittenberg, N. J.; Oh, S. H.; Cho, N. J. Plasmonic Nanohole Sensor for Capturing Single Virus-like Particles toward Virucidal Drug Evaluation. *Small* **2016**, *12*, 1159−1166.

(12) Nakatsuka, N.; Yang, K.-A.; Abendroth, J. M.; Cheung, K. M.; Xu, X.; Yang, H.; Zhao, C.; Zhu, B.; Rim, Y. S.; Yang, Y.; et al. Aptamer−Field-Effect Transistors Overcome Debye Length Limitations for Small-Molecule Sensing. *Science* **2018**, *362*, 319−324.

(13) Christensen, S. M.; Stamou, D. Surface-Based Lipid Vesicle Reactor Systems: Fabrication and Applications. *Soft Matter* **2007**, *3*, 828−836.

(14) Christensen, S. M.; Stamou, D. G. Sensing-Applications of Surface-Based Single Vesicle Arrays. *Sensors* **2010**, *10*, 11352−11368.

DOI: 10.1021/acsami.9b01724
ACS Appl. Mater. Interfaces 2019, 11, 13984−13990

(15) Tabaei, S. R.; Rabe, M.; Zhdanov, V. P.; Cho, N.-J.; Höök, F. Single Vesicle Analysis Reveals Nanoscale Membrane Curvature Selective Pore Formation in Lipid Membranes by an Antiviral α-Helical Peptide. *Nano Lett.* **2012**, *12*, 5719−5725.
(16) Jackman, J. A.; Saravanan, R.; Zhang, Y.; Tabaei, S. R.; Cho, N. J. Correlation between Membrane Partitioning and Functional Activity in a Single Lipid Vesicle Assay Establishes Design Guidelines for Antiviral Peptides. *Small* **2015**, *11*, 2372−2379.
(17) Jackman, J. A.; Costa, V. V.; Park, S.; Real, A. L. C.; Park, J. H.; Cardozo, P. L.; Ferhan, A. R.; Olmo, I. G.; Moreira, T. P.; Bambirra, J. L.; et al. Therapeutic Treatment of Zika Virus Infection Using a Brain-Penetrating Antiviral Peptide. *Nat. Mater.* **2018**, *17*, 971.
(18) Zan, G. H.; Jackman, J. A.; Cho, N.-J. AH Peptide-Mediated Formation of Charged Planar Lipid Bilayers. *J. Phys. Chem. B* **2014**, *118*, 3616−3621.
(19) Liu, Z.; Qiao, J.; Niu, Z.; Wang, Q. Natural Supramolecular Building Blocks: From Virus Coat Proteins to Viral Nanoparticles. *Chem. Soc. Rev.* **2012**, *41*, 6178−6194.
(20) Sanjuán, R. Collective Properties of Viral Infectivity. *Curr. Opin. Virol.* **2018**, *33*, 1−6.
(21) Andreu-Moreno, I.; Sanjuán, R. Collective Infection of Cells by Viral Aggregates Promotes Early Viral Proliferation and Reveals a Cellular-Level Allee Effect. *Curr. Biol.* **2018**, *28*, 3212−3219.
(22) Leeks, A.; Sanjuán, R.; West, S. A. The Evolution of Collective Infectious Units in Viruses. *bioRxiv* **2019**, No. 524694.
(23) Cuevas, J. M.; Durán-Moreno, M.; Sanjuán, R. Multi-Virion Infectious Units Arise from Free Viral Particles in an Enveloped Virus. *Nat. Microbiol.* **2017**, *2*, 17078.
(24) Chen, Y.-H.; Du, W.; Hagemeijer, M. C.; Takvorian, P. M.; Pau, C.; Cali, A.; Brantner, C. A.; Stempinski, E. S.; Connelly, P. S.; Ma, H.-C.; et al. Phosphatidylserine Vesicles Enable Efficient En bloc Transmission of Enteroviruses. *Cell* **2015**, *160*, 619−630.
(25) Santiana, M.; Ghosh, S.; Ho, B. A.; Rajasekaran, V.; Du, W.-L.; Mutsafi, Y.; De Jésus-Diaz, D. A.; Sosnovtsev, S. V.; Levenson, E. A.; Parra, G. I.; et al. Vesicle-Cloaked Virus Clusters are Optimal Units for Inter-Organismal Viral Transmission. *Cell Host Microbe* **2018**, *24*, 208−220.
(26) Münch, J.; Rücker, E.; Ständker, L.; Adermann, K.; Goffinet, C.; Schindler, M.; Wildum, S.; Chinnadurai, R.; Rajan, D.; Specht, A.; et al. Semen-Derived Amyloid Fibrils Drastically Enhance HIV Infection. *Cell* **2007**, *131*, 1059−1071.
(27) Wallis, C.; Melnick, J. L. Virus Aggregation as the Cause of the Non-Neutralizable Persistent Fraction. *J. Virol.* **1967**, *1*, 478−488.
(28) Gerba, C. P.; Betancourt, W. Q. Viral Aggregation: Impact on Virus Behavior in the Environment. *Environ. Sci. Technol.* **2017**, *51*, 7318−7325.
(29) Edelhoch, H. Spectroscopic Determination of Tryptophan and Tyrosine in Proteins. *Biochemistry* **1967**, *6*, 1948−1954.
(30) Biswas, K. H.; Jackman, J. A.; Park, J. H.; Groves, J. T.; Cho, N.-J. Interfacial Forces Dictate the Pathway of Phospholipid Vesicle Adsorption onto Silicon Dioxide Surfaces. *Langmuir* **2018**, *34*, 1775−1782.
(31) Bernard, A.; Renault, J. P.; Michel, B.; Bosshard, H. R.; Delamarche, E. Microcontact Printing of Proteins. *Adv. Mater.* **2000**, *12*, 1067−1070.
(32) Huang, N.-P.; Michel, R.; Voros, J.; Textor, M.; Hofer, R.; Rossi, A.; Elbert, D. L.; Hubbell, J. A.; Spencer, N. D. Poly(L-lysine)-g-poly(ethylene glycol) Layers on Metal Oxide Surfaces: Surface-analytical Characterization and Resistance to Serum and Fibrinogen Adsorption. *Langmuir* **2001**, *17*, 489−498.
(33) Ruiz, S. A.; Chen, C. S. Microcontact Printing: A Tool to Pattern. *Soft Matter* **2007**, *3*, 168−177.
(34) Csucs, G.; Michel, R.; Lussi, J. W.; Textor, M.; Danuser, G. Microcontact Printing of Novel Co-Polymers in Combination with Proteins for Cell-Biological Applications. *Biomaterials* **2003**, *24*, 1713−1720.
(35) Lohse, B.; Bolinger, P.-Y.; Stamou, D. Encapsulation Efficiency Measured on Single Small Unilamellar Vesicles. *J. Am. Chem. Soc.* **2008**, *130*, 14372−14373.
(36) Bernard, A.; Delamarche, E.; Schmid, H.; Michel, B.; Bosshard, H. R.; Biebuyck, H. Printing Patterns of Proteins. *Langmuir* **1998**, *14*, 2225−2229.
(37) Cao, H. H.; Nakatsuka, N.; Serino, A. C.; Liao, W.-S.; Cheunkar, S.; Yang, H.; Weiss, P. S.; Andrews, A. M. Controlled DNA Patterning by Chemical Lift-Off Lithography: Matrix Matters. *ACS Nano* **2015**, *9*, 11439−11454.
(38) Abendroth, J. M.; Nakatsuka, N.; Ye, M.; Kim, D.; Fullerton, E. E.; Andrews, A. M.; Weiss, P. S. Analyzing Spin Selectivity in DNA-Mediated Charge Transfer via Fluorescence Microscopy. *ACS Nano* **2017**, *11*, 7516−7526.
(39) Eloul, S.; Compton, R. G. General Model of Hindered Diffusion. *J. Phys. Chem. Lett.* **2016**, *7*, 4317−4321.
(40) Dieteren, C. E.; Gielen, S. C.; Nijtmans, L. G.; Smeitink, J. A.; Swarts, H. G.; Brock, R.; Willems, P. H.; Koopman, W. J. Solute Diffusion is Hindered in the Mitochondrial Matrix. *Proc. Natl. Acad. Sci. USA* **2011**, *108*, 8657−8662.
(41) Cho, N.-J.; Dvory-Sobol, H.; Xiong, A.; Cho, S.-J.; Frank, C. W.; Glenn, J. S. Mechanism of an Amphipathic α-Helical Peptide's Antiviral Activity Involves Size-Dependent Virus Particle Lysis. *ACS Chem. Biol.* **2009**, *4*, 1061−1067.
(42) Jackman, J. A.; Zan, G. H.; Zhdanov, V. P.; Cho, N.-J. Rupture of Lipid Vesicles by a Broad-Spectrum Antiviral Peptide: Influence of Vesicle Size. *J. Phys. Chem. B* **2013**, *117*, 16117−16128.
(43) Hanson, J. M.; Gettel, D. L.; Tabaei, S. R.; Jackman, J.; Kim, M. C.; Sasaki, D. Y.; Groves, J. T.; Liedberg, B.; Cho, N.-J.; Parikh, A. N. Cholesterol-Enriched Domain Formation Induced by Viral-Encoded, Membrane-Active Amphipathic Peptide. *Biophys. J.* **2016**, *110*, 176−187.

DOI: 10.1021/acsami.9b01724
ACS Appl. Mater. Interfaces 2019, 11, 13984−13990